

Tryptophan UV Resonance Raman Excitation Profiles

Joyce A. Sweeney and Sanford A. Asher*

Department of Chemistry, University of Pittsburgh, Pittsburgh, Pennsylvania 15260

(Received: September 19, 1989)

We report the first quantitative UV resonance Raman excitation profiles of tryptophan (Trp) in the spectral region between 207 and 250 nm. The Trp excitation profiles are narrow and show maxima at ca. 224 nm which are 4 nm red-shifted from the ca. 220-nm B_b absorption band maximum. The excitation profile band shapes indicate that Trp can be selectively enhanced in proteins. We see destructive interference between the ca. 195-nm B_a and the 220-nm B_b electronic transitions. This destructive interference bestows a spectral window at ca. 205 nm with little Trp enhancement, thus permitting selective ca. 205-nm-excitation studies of protein amide modes to examine protein secondary structure. We use the Raman intensity data to examine excited-state Trp geometry changes relative to the ground state. We detail the UV photophysics of Trp and describe the energy flux conditions appropriate for studying ground-state Trp species. Our Trp excitation profiles dramatically differ from those of Fodor et al. (*J. Am. Chem. Soc.* **1989**, *111*, 5509) because we avoid the high pulse energy flux conditions which both depopulate the Trp ground-state concentration and excite the Raman spectra of transient photochemical species.

Introduction

The development of UV resonance Raman spectroscopy as a new technique for studying molecular structure of both ground-state and excited-state species will be of unique importance for studies of biological macromolecules.¹ It is possible to selectively examine the vibrational spectra of isolated chromophores such as aromatic amino acids in proteins, for example. We, as well as others,¹⁻¹¹ have focused on developing a fundamental understanding of the phenomenology of resonance Raman enhancement for small molecules such as the aromatic amino acids as well as for amides and peptides. We have also concentrated on clarifying the accompanying photochemical and photophysical phenomena, in order to ensure that the spectroscopic data are clearly interpretable as due to either ground- or excited-state species.^{3,12a,b}

We previously had reported qualitative Trp excitation profiles³ which, as we stated, were compromised by photochemistry and Raman saturation. In addition, Spiro and co-workers⁹ recently reported a coarse excitation profile study which, as we demonstrate here, is incorrect due to Raman saturation and Raman scattering from photochemical intermediates. Our work reported here avoids Raman saturation and photochemistry and is the first resonance Raman excitation profile study of tryptophan to give accurate Raman cross sections. We utilize the excitation profiles to examine Trp excited-state structure. We see narrow excitation profiles which are red-shifted relative to the B_b absorption band maximum. The narrowness of the profiles augurs well for selective enhancement of Trp residues in proteins. We see destructive interference on the blue side of the 220-nm absorption band; this destructive interference bestows a spectral window for studies of amide backbone vibrations at ca. 205 nm. This study represents the conclusion of the preliminary studies required for the quantitative use of Raman intensities to monitor aromatic amino acid environments in proteins.

Experimental Section

The 1.0 mM tryptophan (Sigma Chemical Co.) aqueous sample solutions contained 1.0 M sodium perchlorate (Aldrich Chemical Co.) as the internal intensity standard. The high pH samples were maintained at pH 11.5 to ensure deprotonation of the amino and carboxyl groups. Approximately 10 mL of sample solutions was recirculated through a 1.0 mm i.d. Suprasil quartz capillary tube by a magnetic gear pump. Samples were replaced after each spectral measurement and the maximum irradiation time was 15 min.

The laser excitation source utilized a Quanta-Ray DCR-2A Nd:YAG laser in which the 1.06- μ m fundamental was frequency doubled to pump a dye laser which emitted 4-6-ns pulses at a 20-Hz repetition rate. The dye laser output was frequency doubled

and mixed with the YAG fundamental to generate excitation frequencies between 217 and 250 nm. Excitation wavelengths between 207 and 215 nm were generated by a XeCl excimer laser system. The 308-nm fundamental of a 200-Hz Lambda-Physik Model EMG 103 excimer laser excited a Lambda-Physik Model FL 3002 dye laser, and the dye laser output was frequency doubled with a β -barium borate doubling crystal. The defocused laser beam (beam diameter = 2 mm at the sample) excited the sample in the capillary tube. An ellipsoidal mirror collected the 90° scattered light and focused this light onto the entrance slit of a Spex Triplemate spectrometer. A crystalline quartz wedge randomized the polarization of light entering the spectrometer to avoid any polarization efficiency bias of the monochromator. The spectrometer has been detailed elsewhere.^{13,14} The spectrograph stage of the Triplemate monochromator equipped with a 1200 groove/mm grating gave a spectral resolution of ca. 29 cm^{-1} at 220 nm and ca. 24 cm^{-1} at 240 nm with the 200- μ m slit width used. A Princeton Applied Research Model 1215 OMA II data station interfaced to an EG&G PAR Model 1420 blue-intensified Reticon was used to detect the dispersed light. We determined the throughput efficiencies of the spectrometer and detector in the UV wavelength region by using a standard intensity deuterium lamp scattered from a Lambert surface prepared from Kodak White Reflectance Standard.

The peak widths in the observed spectra are dominated by the instrument band-pass. Thus, in the absence of spectral congestion, essentially identical peak band shapes will be observed for the tryptophan and the internal intensity standard Raman bands.¹⁵

(1) Asher, S. A. *Annu. Rev. Phys. Chem.* **1988**, *39*, 537.

(2) Johnson, C. R.; Ludwig, M.; O'Donnell, S.; Asher, S. A. *J. Am. Chem. Soc.* **1984**, *106*, 5008.

(3) Asher, S. A.; Ludwig, M.; Johnson, C. R. *J. Am. Chem. Soc.* **1986**, *108*, 3186.

(4) Rava, R. P.; Spiro, T. G. *J. Phys. Chem.* **1985**, *89*, 1856.

(5) Fodor, S. P. A.; Rava, R. P.; Hays, T. R.; Spiro, T. G. *J. Am. Chem. Soc.* **1985**, *107*, 1520.

(6) Dudik, J. M.; Johnson, C. R.; Asher, S. A. *J. Phys. Chem.* **1985**, *89*, 3805.

(7) Mayne, L. C.; Ziegler, L. D.; Hudson, B. S. *J. Phys. Chem.* **1985**, *89*, 3395.

(8) (a) Rava, R. P.; Spiro, T. G. *Biochemistry* **1985**, *24*, 1861. (b) Copeland, R. A.; Dasgupta, S.; Spiro, T. G. *J. Am. Chem. Soc.* **1985**, *107*, 3370.

(9) Fodor, S. P. A.; Copeland, R. A.; Gryon, C. A.; Spiro, T. G. *J. Am. Chem. Soc.* **1989**, *111*, 5509.

(10) (a) Song, S.; Asher, S. A.; Krimm, S.; Bandekar, J. *J. Am. Chem. Soc.* **1988**, *110*, 8547. (b) Song, S.; Asher, S. A. *J. Am. Chem. Soc.* **1989**, *111*, 4295. (c) Krimm, S.; Song, S.; Asher, S. A. *J. Am. Chem. Soc.* **1989**, *111*, 4290.

(11) Ludwig, M.; Asher, S. A. *J. Am. Chem. Soc.* **1988**, *110*, 1005.

(12) (a) Teraoka, J.; Harmon, P.; Asher, S. A. *J. Am. Chem. Soc.* **1990**, *112*, 2892. (b) Johnson, C. R.; Ludwig, M.; Asher, S. A. *J. Am. Chem. Soc.* **1986**, *108*, 905.

(13) Asher, S. A.; Johnson, C. R.; Murtaugh, J. *Rev. Sci. Instrum.* **1983**, *54*, 1657.

(14) Asher, S. A. *Appl. Spectrosc.* **1984**, *38*, 276.

* Author to whom correspondence should be addressed.

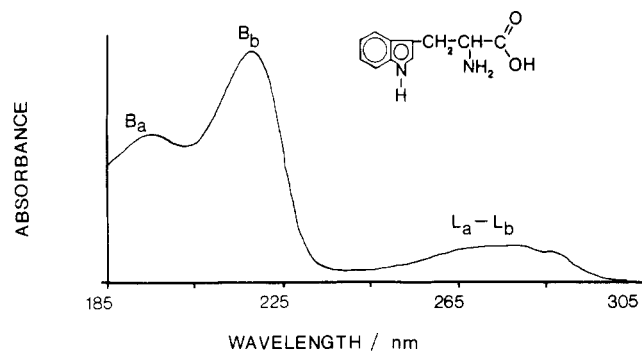


Figure 1. Absorption spectrum of an aqueous solution of tryptophan at pH 7. Concentration: 30 μ M tryptophan.

Therefore, the ratios of peak heights of the tryptophan bands relative to those of the internal intensity standard are identical with the integrated peak intensity ratios; the peak intensity ratios are proportional to total Raman cross section ratios. These peak height ratios, the spectrometer efficiency factors, and the absolute Raman cross sections of the 932- cm^{-1} band of sodium perchlorate previously determined by Dudik et al.¹⁶ were used to calculate the total Raman cross sections for all of the tryptophan bands except for the band at 1345 cm^{-1} . Because this band is actually a broad doublet (1360 and 1342 cm^{-1}) arising from Fermi resonance,¹⁷ the analyte and internal standard band shapes differed. For this case we used peak area ratios to calculate the Raman cross sections. For excitation wavelengths below 217 nm we used ClO_4^- cross sections derived from an Albrecht *A*-term fit using Dudik et al.'s measured parameters.

Self-absorption negligibly affected the relative intensity ratios.¹⁸ We minimized the self-absorption by irradiating the sample capillary at the front surface to optimize the Raman signal. This minimized the path length of the Raman scattered light out of the absorbing sample. The lack of self-absorbance bias was confirmed by comparing the relative intensities of acetonitrile solvent bands at 918, 2249, and 2942 cm^{-1} in both pure acetonitrile and in a sample solution containing 1.0 mM tryptophan in 50% acetonitrile and water. In addition, we also compared 1.0 mM tryptophan spectra obtained from the capillary to those from a backscattering study from a 0.2 mm thick sample jet stream which gives an essentially negligible self-absorption bias of the relative intensity ratios. We conclude after careful study, and in view of our recent self-absorption model calculations,¹⁸ that self-absorption biases the observed relative intensity ratios by less than 5% for the 760- and 1009- cm^{-1} bands and less than 15% for the 1550- cm^{-1} band in the worst case situation (excitation at 218 nm). We expect that the measured Raman cross sections are accurate to better than 20% (2σ). The frequencies reported we expect are accurate to within ± 4 cm^{-1} .

We determined the Raman cross sections at each excitation wavelength by measuring Raman spectra at three different laser pulse energies. Neutral-density filters of varying optical density were used to attenuate the pulse energies. Because the low pulse energies used occur in a linear Raman saturation regime, the Raman cross sections were determined by extrapolating to zero pulse excitation energy.¹² The Raman spectra used for the excitation profiles did not show Raman bands from photochemical intermediates.¹² The lack of absorption spectral changes in response to the laser irradiation demonstrates that negligible sample degradation occurred during the Raman spectral measurements.

Results

The absorption spectrum of tryptophan at pH 7 (Figure 1) shows broad bands at ca. 280, 220, and 195 nm. Alteration in

TABLE I: Tryptophan Absorption Spectral Parameters

electronic transition	λ_{max} , nm		ϵ , $\text{M}^{-1} \text{cm}^{-1}$	
	pH 7	pH 11.5	pH 7	pH 11.5
B_a	194.8		23000	
B_b	217.9	220.4	36000	32000
L_a-L_b	278.0	279.2	5800	5600

TABLE II: Assignments of the Vibrational Modes of Tryptophan

obsd freq, cm^{-1}	assignment ^a		description
	(a)	(b)	
760		W18	symmetric benzene/pyrrole in-phase breathing mode (ref 22)
877	ν_{10a}	W17	indole ring vibration with NH bending (ref 22)
1009		W16	symmetric benzene/pyrrole out-of-phase breathing mode (ref 22)
1345		W7	pyrrole ring vibration (refs 22, 17, 23)
1550		W3	C_2-C_3 stretching mode of the pyrrole ring (refs 17, 23)
1578	ν_{8b}	W2	phenyl mode (refs 17, 23)
1614	ν_{8a}	W1	phenyl mode with some contribution from the pyrrole N_1C_8 stretching (refs 17, 23)

^a From (a) Hirakawa et al.²² and (b) Harada et al.^{17,23}

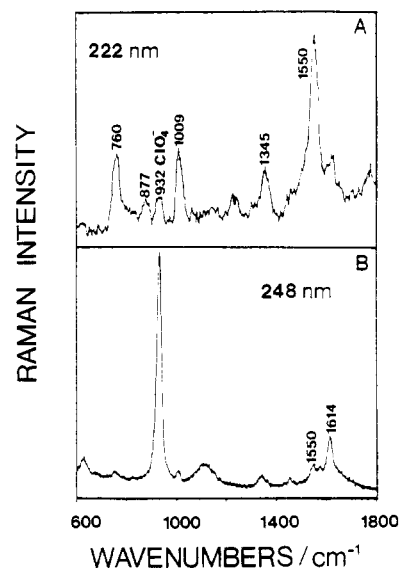


Figure 2. Resonance Raman spectra of tryptophan with excitation at 222 and 248 nm. The band at 932 cm^{-1} derives from ClO_4^- , the internal intensity standard. Concentrations: 1.0 mM Trp and 1.0 M NaClO_4 at pH 11.5. The 222-nm spectrum was obtained with a pulse energy of 1.6 mJ/(pulse- cm^2) and at 248 nm with 4.8 mJ/(pulse- cm^2).

the solution pH results in small λ_{max} and ϵ_{max} absorption spectral changes due to changes in the Trp protonation state (Table I). The ca. 280-nm band derives from two overlapping $\pi \rightarrow \pi^*$ transitions to the L_a and L_b excited states.¹⁹⁻²¹ These L_a and L_b states are related to the ${}^1B_{1u}$ and ${}^1B_{2u}$ excited states of benzene. Although a dipole transition to these states is formally symmetry forbidden in benzene, the decreased symmetry of the substituted phenyl ring results in increased oscillator strengths for transitions to the L_a and L_b states compared to those in benzene.²¹ The maximum molar absorptivity for the overlapping L_a-L_b band for Trp in aqueous solution at pH 7 is 5800 $\text{M}^{-1} \text{cm}^{-1}$. The much stronger $\pi \rightarrow \pi^*$ transitions to the B_a and B_b excited states at 195 and 220 nm have molar absorptivities of 23 000 and 36 000 $\text{M}^{-1} \text{cm}^{-1}$, respectively. The B_a and B_b excited states derive from the splitting of the E_{1u} excited state of benzene due to the reduced

(15) Murtaugh, J.; Asher, S. A. *Appl. Spectrosc.* **1988**, *42*(1), 83.

(16) Dudik, J. M.; Johnson, C. R.; Asher, S. A. *J. Chem. Phys.* **1985**, *82*, 1732.

(17) Harada, I.; Miura, T.; Takeuchi, H. *Spectrochim. Acta* **1986**, *42A* (2/3), 307.

(18) Ludwig, M.; Asher, S. A. *Appl. Spectrosc.* **1988**, *42*(8), 1458.

(19) Creed, D. *Photochem. Photobiol.* **1984**, *39*(4), 537.

(20) Song, P.; Kurtin, W. J. *Am. Chem. Soc.* **1969**, *91*(17), 4892.

(21) Ziegler, L. D.; Hudson, B. S. In *Excited States*; Lim, E. C., Ed.; Academic: New York, 1982; Vol. V, p 41.

ring symmetry. Molar absorptivities and wavelengths of maximum absorption at pH 7 and 11.5 are listed in Table I. The ϵ_{\max} of the B_a transition at pH 11.5 was not obtained due to the OH^- absorbance in this region.

Figure 2 shows resonance Raman spectra of tryptophan excited at 222 and 248 nm. The band assignments which are listed in Table II derive from Hirakawa et al.²² and Harada et al.²³ The prominent bands at 760 and 1009 cm^{-1} are due to coupled vibrations which involve the ν_1 symmetric ring stretching of the benzene ring and the symmetric ring stretching of the pyrrole ring.²² These two modes couple in and out of phase to produce the 760- and 1009- cm^{-1} bands, respectively. The 877- cm^{-1} band, ν_{10a} , is an in-plane indole vibration with a contribution from an NH in-plane deformation. The broad 1345- cm^{-1} band is very sensitive to local environment because it derives from a Fermi resonance which involves the fundamental N_1-C_8 stretching mode of the indole ring (W7) and combinations of out-of-plane indole ring bending vibrations (W25 + W33 and/or W28 + W29).^{17,23} On the basis of the recent normal vibrational coordinate study of Harada et al.²³ we now agree with the conclusion of Fodor et al.⁹ and reassign the 1550- cm^{-1} band to a vibration labeled W3 which mainly involves C_2-C_3 stretching of the pyrrole ring with some C-H in-plane bending in both the phenyl and pyrrole rings.²³ We, thus, now conclude that the bands at 1578 and 1614 cm^{-1} derive from the ν_{8b} and ν_{8a} modes of benzene, respectively.

We previously showed that the 1578- cm^{-1} vibration is the most intense feature upon excitation at 273 nm in resonance with the L_a-L_b excited states.³ For the excitation wavelength range employed in this study (207–250 nm), this band is strongly enhanced only with excitation at greater than 247 nm. The 1550- cm^{-1} band dominates the Raman spectra for excitation between 207 and 236 nm as evident from the 2-fold greater intensity of the RREP maximum for this band compared to the 760-, 1009-, and 1345- cm^{-1} bands (Figure 3). The normal-coordinate analysis by Harada et al. shows that the 1550- cm^{-1} band derives mainly from a pyrrole mode which is dominated by the C_2-C_3 stretching in the pyrrole ring.¹⁷⁻²³ According to Song and Kurtin,²⁰ the B_b transition shows a large transition moment approximately along the long axis of the indole ring, bisecting the C_6 carbon and the C_2-C_3 bond. This indicates²⁴ that excitation within this $\pi \rightarrow \pi^*(B_b)$ transition results in a large change in the electron density about the C_2-C_3 bond which results in a localized bond length change. Thus, the 1550- cm^{-1} vibration with a large component of C_2-C_3 stretching will be especially enhanced. Thus, we agree with the theoretical calculation and conclude that the geometric alteration of the B_b excited state compared to the ground state involves an overall distortion of the indole ring, with a pronounced elongation or compression of the C_2-C_3 bond, accompanied by changes in the C_5-C_6 and C_6-C_7 bond lengths. We expect significant enhancement of the ring breathing modes at 760 and 1009 cm^{-1} , because they are delocalized over the indole ring.

The 1550- and 1614- cm^{-1} bands show similar intensities at 238-nm excitation, but with excitation at ca. 240 nm the ν_{8a} 1614- cm^{-1} band dominates the spectrum (Figure 2b). The 932- cm^{-1} band in all of the Raman spectra derives from the perchlorate internal intensity standard.

We previously reported "qualitative" excitation profiles of Trp which we indicated were severely compromised by Raman saturation.³ In the present study here we determined the Raman cross sections by working at extremely low pulse energies and by extrapolating our intensity data to zero pulse energies.^{12,25} We previously demonstrated that the ratio of intensities of the tryptophan bands to the internal intensity standard band strongly

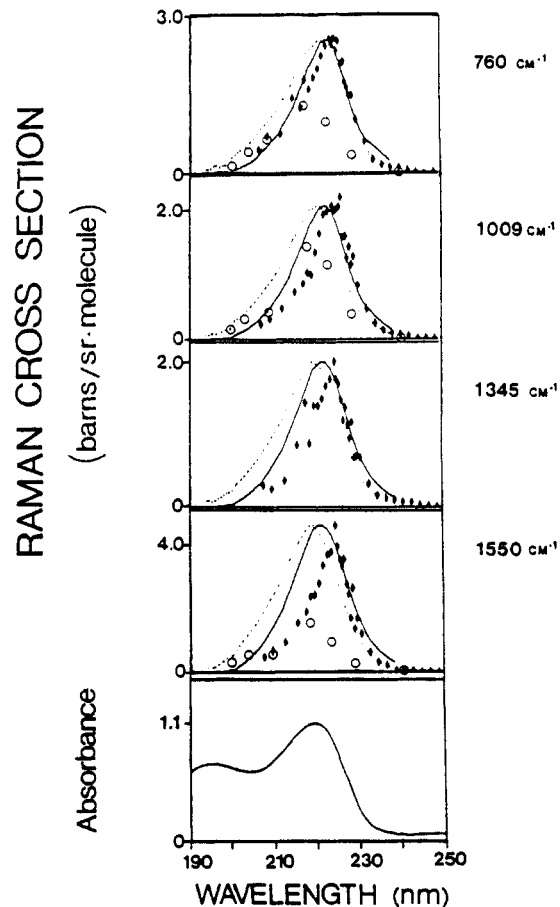


Figure 3. Resonance Raman excitation profiles of vibrational modes of Trp. The experimental data (diamonds) are red-shifted 4 nm from the absorption maximum of the B_b transition. The broken curve represents the basic Condon transform calculation of the RREP. The solid curve is the result of introducing non-Condon coupling into the transform calculation. See text for details. The data shown by open circles are from Fodor et al.⁹

depend upon incident pulse energy due to depletion of the ground-state population by absorption.¹² The B_b excited tryptophan molecules may undergo photoionization or photochemistry or directly relax into the long-lived L_a-L_b states.^{12a} Since only ground-state molecules give rise to Raman scattering, a simple three-state model gives a Raman intensity dependence of^{12,25}

$$I_p = W \frac{\sigma_p P_0 I_0}{\sigma_A} [1 - e^{-\sigma_A I_0}] \quad (1)$$

where I_p is the analyte Raman intensity integrated over the time of the laser pulse, σ_p is the analyte Raman cross section, σ_A is the analyte absorbance cross section, P_0 is the initial ground-state analyte population and I_0 is the total number of photons within the laser pulse. The product $\sigma_A I_0$ is the relative probability of photon absorption. W is an instrumental parameter which monitors the efficiency of Raman light detection. When $\sigma_A I_0 \ll 1$, the leading terms approximate the exponential series. Thus, a linear Raman laser pulse energy dependence is expected at low energy fluxes.

$$I_p \cong W \sigma_p P_0 I_0 \left[1 - \frac{\sigma_A I_0}{2} \right] \quad (2)$$

The internal standard does not absorb in the spectral region of interest; its ground-state population is independent of energy flux. Thus, its Raman intensity is simply proportional to incident laser flux

$$I_S = W \sigma_S C_S I_0 \quad (3)$$

where C_S is the internal standard concentration. The relative ratio,

(22) Hirakawa, A. Y.; Nishimura, Y.; Tudashi, M.; Nakanishi, M.; Tsuboi, M. *J. Raman Spectrosc.* **1978**, *7*, 282.

(23) Harada, I.; Takeuchi, H. In *Spectroscopy of Biological Systems*; Clark, R. J. H., Hester, R. E., Eds.; Wiley: New York, 1986; Vol. 13, p 157.

(24) Longuet-Higgins, H. C. *Proc. R. Soc. (London) Ser. A* **1956**, *235*, 537.

(25) Jones, C. M.; Devito, V. L.; Harmon, P. A.; Asher, S. A. *Appl. Spectrosc.* **1987**, *41*(8), 1268.

(26) Harmon, P. A., personal communication.

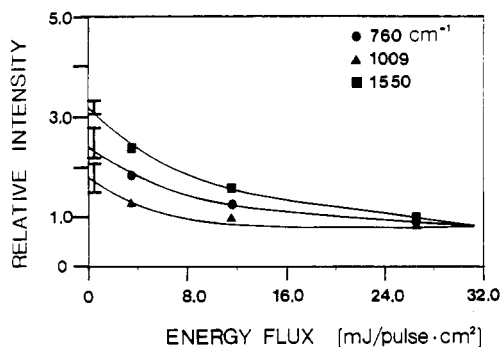


Figure 4. The incident energy flux dependence of the relative intensities of Trp bands to the 932-cm⁻¹ internal intensity standard band of perchlorate. The error bars represent the extrapolated relative intensity ratios at zero incident energy flux obtained from three different data sets.

R , of analyte Raman intensity to internal standard intensity at low laser powers is

$$R = \frac{I_p}{I_s} = \frac{\sigma_p P_0}{\sigma_s C_s} \left[1 - \frac{\sigma_A I_0}{2} \right] \quad (4)$$

and

$$\lim_{I_0 \rightarrow 0} R = \frac{\sigma_p P_0}{\sigma_s C_s} \quad (5)$$

This dependence of the experimental relative intensity ratios on incident pulse energy flux has been documented previously¹² and is coarsely illustrated in Figure 4 which at low fluxes shows a linear decrease in the Trp relative intensities. The relative intensity ratios extrapolated to zero incident energy flux are the true Raman cross sections.

This simple saturation model assumes no relaxation of excited tryptophan molecules back to the ground state within the laser pulse. The Raman intensities of all of the tryptophan bands should saturate identically and the intensity ratios of the Trp bands relative to one another must remain constant, independent of incident energy flux. If the relative intensities are found to depend upon pulse energy, additional phenomena must be occurring.

We earlier demonstrated at 235-nm excitation that for sufficiently high energy fluxes, photochemical intermediates (probably S_1) give rise to new bands.¹² Figure 5 demonstrates the energy flux dependence of the formation of the intermediates for 218-nm excitation. At the lowest flux energy we observe a spectrum essentially that of ground-state Trp. A 3-fold increase in excitation flux yields a spectrum with an increased intensity for the 760- and 1009-cm⁻¹ bands compared to the 1550-cm⁻¹ band. The difference spectrum shown in Figure 5D clearly illustrates the bands which derive from photochemical intermediates. The pulse energy dependence of the relative intensities in the Raman spectra seems to saturate at pulse energies between those used for Figure 5B and Figure 5C. At higher fluxes a steady-state concentration appears to occur. The intensity decreases for the 760- and 1009-cm⁻¹ bands which result from depopulation of the ground state are essentially cancelled by the increased intensities which derive from the photochemical intermediate species (Figure 4).

Figure 4 shows the relative intensity dependence upon laser energy flux for three of the Trp bands at 760, 1009, and 1550 cm⁻¹. At low energy fluxes (i.e., less than ca. 10 mJ/(pulse·cm²)) the tryptophan intensities all decrease together with increasing flux. However, above ca. 10 mJ/(pulse·cm²), the rate of decrease slows, the band intensities decrease differently, and the relative ratios change. Above 25 mJ/(pulse·cm²) Raman intensities become almost independent of energy flux, and the intensities of the Trp bands converge.

Figure 3 shows our experimental resonance Raman excitation profiles (RREP's) of the 760-, 1009-, 1345-, and 1550-cm⁻¹ bands of Trp at pH 11.5 (diamonds). These excitation profiles all peak at 224 nm and are red-shifted by 4 nm from the absorption maximum of the resonant B_0 electronic transition at 220 nm. The

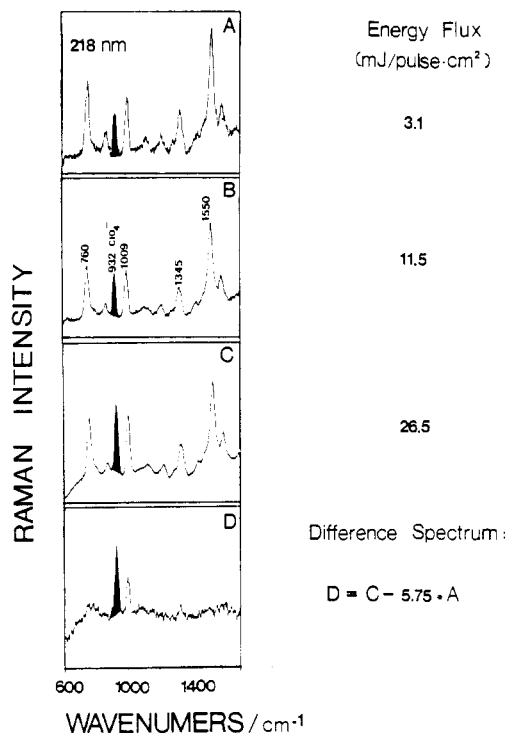


Figure 5. Raman spectra of tryptophan with excitation at 218 nm and incident energy fluxes of (A) 3.5, (B) 11.5, and (C) 26.5 mJ/(pulse·cm²). (D) The difference spectrum of (C - A) utilizes a scaling factor that removes the contribution of ground-state tryptophan. The difference spectrum displays transient bands at ca. 760 and 1009 cm⁻¹. The shaded band at 932 cm⁻¹ in all of the spectra derives from the symmetric stretch of the intensity standard, perchlorate, which is observed because it does not saturate and does not cancel with the scaling factor used for the difference spectra. These spectra have not been corrected for spectrometer efficiency.

TABLE III: Total Differential Raman Cross Sections for the 760, 1009, 1345, and 1550 cm⁻¹ Totally Symmetric Vibrational Modes of Tryptophan at pH 11.5

excitation wavelength, nm	total differential Raman cross section, barns/(molecule·sr)			
	760 cm ⁻¹	1009 cm ⁻¹	1345 cm ⁻¹	1550 cm ⁻¹
207	0.42	0.23	0.31	0.51
215	1.41	0.72	0.88	1.55
218	1.74	1.04	1.28	2.37
220	1.79	1.31	1.42	2.74
222	2.20	1.89	1.70	3.60
224	2.52	2.02	2.04	4.51
226	2.48	1.50	1.22	3.47
228	1.60	1.40	1.20	2.60
230	1.00	0.82	0.70	1.20
240	0.091	0.084	0.077	0.11
250	0.012	0.016	0.020	0.040

bandwidths of the RREP's are ca. 11 nm and are narrower than the apparent bandwidth of the resonant B_0 transition of ca. 17 nm. Tables III and IV show the Raman cross sections for Trp solutions at pH 11.5 and pH 7 at a number of excitation wavelengths. The small cross-section differences between the different pH samples arise from the absorption spectral changes which occur as indicated in Table I. Our measured Trp Raman cross sections, which are listed in Tables III and IV and displayed in Figure 3, differ from those recently reported by Spiro and co-workers.⁹ This is clearly evident from Figure 3 in which we also plot the cross-section data of Spiro and co-workers by the open circles. We conclude that their data are influenced by Raman saturation and contributions from Raman bands of excited-state species caused by the use of too high pulse energies in the measurements.

These conclusions appear unequivocal on the basis of the following considerations: (1) Our cross sections are systematically larger. In fact, at 223 nm which is close to the excitation profile

TABLE IV: A Comparison of Trp Total Differential Raman Cross Sections at pH 7 and pH 11.5 (barns/(molecule-sr))

excitation wavelength, nm	760 cm ⁻¹		1009 cm ⁻¹		1550 cm ⁻¹	
	pH 11.5	pH 7	pH 11.5	pH 7	pH 11.5	pH 7
218	1.74 ± 0.17	1.84	1.04	1.31	2.37 ± 0.14	2.94 ± 0.21
223	2.24 ± 0.10	2.72 ± 0.15	1.84 ± 0.07	2.21 ± 0.14	3.06 ± 0.15	3.09 ± 0.14
225 ^a		2.1				2.2
227	1.99 ± 0.10	1.69 ± 0.17	1.56 ± 0.06	1.34 ± 0.16	2.30 ± 0.08	1.60 ± 0.08

^a From ref 26.

maximum, our cross sections for the 1550-cm⁻¹ band are more than 3-fold greater. As indicated in Table IV, although changes occur in the cross section between pH 7 and pH 11.5 Trp solutions, the changes are modest and do not account for the dramatic differences between the Trp pH 7 data of Fodor et al. and our pH 11.5 data. A decrease in the "apparent" cross sections results from ground-state depletion. (2) Our Raman cross sections for the 760- and 1009-cm⁻¹ bands are significantly less than those of the 1550-cm⁻¹ band for excitation well in resonance, in contrast to the results of Fodor et al.⁹ who report similar cross sections for the 760-, 1009-, and 1550-cm⁻¹ bands. From our Figure 4 and Figure 5 studies of the pulse energy dependence of the Trp Raman spectra it is clear that photochemical transients contribute to the intensity of the 760- and 1009-cm⁻¹ bands under saturation excitation conditions; this would yield their relative cross section ratios. (3) They did not observe a strongly peaked excitation profile; saturation can dramatically broaden the apparent excitation profile.¹¹ (4) Although Fodor et al. demonstrated experimentally that their relative intensities were essentially independent of the excitation pulse energy, we conclude that they measured this energy dependence in a region of extensive saturation where little further dependence upon pulse energy occurs. This saturation behavior is illustrated by our previous results as well as the Trp saturation curve of Figure 4. The pulse energy independence of Fodor et al.'s cross sections at low energy flux, and the precipitous plummet at higher fluxes is inconsistent with normal Raman saturation which requires a smooth exponential decrease. In the absence of information on their pulse energies, we assume that the plummet at high pulse energies results from higher order nonlinear optical phenomena which turn on at these high pulse energies.

Our cross sections become similar to those of Fodor et al. below 209-nm excitation presumably because their lower available pulse energies prevent extensive saturation. While we expect our values to converge in regions of low Trp absorption at longer excitation wavelengths, our values continue to differ. Presumably this occurs because they utilize even larger pulse energies. Another source of deviation occurs because Fodor et al. inexplicably use SO₄²⁻ internal standard Raman cross section values which they obtained from an Albrecht *A*-term fit of their experimental internal standard cross-section measurements, instead of using their directly measured values. This causes systematic errors in their calculated Trp cross sections measured at wavelengths longer than 229 nm since, in this region, their simple *A*-term model deviates significantly from their more accurate measured values.

Discussion

The surprisingly sharp Trp excitation profiles will be of great utility for selectively enhancing the Raman spectra of Trp residues in proteins. Since the cross sections are likely to depend upon environment and because the excitation profile maxima are likely to shift depending upon the environment it is important to understand the factors which give the observed sharp excitation profiles and the large red shifts of the excitation profile maxima relative to the absorption maximum.

Resonance Raman excitation results in the selective enhancement of those vibrational modes which are vibronically active within the resonant electronic transition. Totally symmetric tryptophan vibrations will be predominantly enhanced via an *A*-term (Franck-Condon) Raman scattering mechanism. For a strongly allowed electronic transition, such as the ¹B₀ ← ¹A₁ transition of tryptophan, the observed Raman intensities provide

information on the resonant excited state, since the degree of enhancement of a given vibration is related to differences in the excited-state geometry, and bond force constants. Further, the Raman excitation profiles (RREP) can be used to predict the optimum excitation wavelengths necessary for enhancing particular vibrational modes of chromophoric segments of macromolecules in order to study molecular structure of complex proteins.

The RREP's in Figure 3 display the dependence of the total differential Raman cross sections upon the laser excitation wavelength. The total Raman scattering cross section, σ_{mn}, for the Raman vibrational transition, n ← m, integrated over 4π sr for an isolated molecule averaged over all orientations is^{3,16,27-31}

$$\sigma_{mn} = \frac{I_{mn}}{I_0} = \frac{27\pi^5}{3^2} \nu_0(\nu_0 - \nu_{mn})^3 GF(T) \left| \sum_{\rho\sigma} \alpha_{\rho\sigma}(\nu_0) \right|^2 \quad (6)$$

*I*_{mn} is the integrated Raman scattered intensity (photons/(s-cm²)) over 4π sr integrated over the bandwidth of the vibrational transition, n ← m. *I*₀ and ν₀ are the incident excitation beam intensity and frequency (cm⁻¹), while ν_{mn} is the frequency of the Raman vibrational mode (cm⁻¹). *G* is a factor specifying the degeneracy of the initial state, *m*, while *F*(*T*) is the Boltzmann weighting factor which determines thermal occupancy of the initial state. α_{ρσ}(ν₀) is the ρ,σth (ρ,σ = x,y,z) component of the Raman polarizability tensor averaged over all molecular orientations at excitation frequency, ν₀.

For 90° Raman scattering measurements from a solution where the incident light is polarized perpendicular to the scattering plane, and both the parallel and perpendicular scattering polarizations are collected, the total differential Raman scattering cross section, σ_R, is given by^{16,29-33}

$$\sigma_R = \frac{d\sigma_{mn}(\nu_0)}{d\Omega}$$

$$\sigma_R = \frac{2^4\pi^4}{45} b^2 G \frac{L\nu_0(\nu_0 - \nu_{mn})^3}{1 - \exp(-hc\nu/kT)} (45\alpha^2 + 7\gamma^2 + 5\delta^2) \quad (7)$$

where *b* is the zero-point vibrational amplitude

$$b = (h/8\pi c^2 \nu_{mn})^{1/2} \quad (8)$$

α², γ², and δ² are the isotropic, anisotropic, and antisymmetric invariants of the polarizability tensor, and *h*, *c*, *k*, and *T* are Planck's constant, the speed of light, Boltzmann's constant, and the temperature, respectively. *L* is the local field correction for the condensed-phase sample and specifies the increased electric field amplitude in the sample over that which would be present in the gas phase.^{29,34}

The components of the polarizability tensor, α_{ρσ}, are given by second-order perturbation theory^{27,35} (eq 9), where ρ and σ are

(27) Tang, J.; Albrecht, A. C. In *Raman Spectroscopy, Theory and Practice*; Szymanski, H. A., Ed.; Plenum: New York, 1970; Vol. II, p 33.

(28) Albrecht, A. C.; Hutley, M. C. *J. Chem. Phys.* **1971**, *55*, 4438.

(29) Schrotter, H. W.; Klochner, H. W. In *Topics in Current Physics*; Weber, A., Ed.; Springer-Verlag: Berlin, 1979; p 123.

(30) Eckhardt, G.; Wagner, W. G. *J. Mol. Spectrosc.* **1977**, *6*, 38.

(31) Mortensen, O. S.; Hassing, S. In *Advances in Infrared and Raman Spectroscopy*; Clark, R. J. H., Hester, R. E., Eds.; Heyden: London, 1980; Vol. 6, p 1.

(32) Skinner, J. G.; Nilsen, W. G. *J. Opt. Soc. Am.* **1968**, *58*, 113.

(33) Long, D. A. In *Raman Spectroscopy*; McGraw Hill: New York, 1977.

(34) Abe, N.; Wakayama, M.; Ito, M. *J. Raman Spectrosc.* **1977**, *6*, 38.

molecular coordinates which label the components of the polarizability tensor. R_σ is the electric dipole moment operator along the molecular coordinate, σ .

$$\alpha_{\rho\sigma} = \sum_{ev} \frac{\langle gm|R_\sigma|ev\rangle\langle ev|R_\rho|gn\rangle}{\nu_{ev} - \nu_m - \nu_0 - i\Gamma_{ev}} + \frac{\langle gm|R_\rho|ev\rangle\langle ev|R_\sigma|gn\rangle}{\nu_{ev} - \nu_n + \nu_0 - i\Gamma_{ev}} \quad (9)$$

ν_{ev} is the transition frequency from the ground state to the ν th vibrational level of the excited electronic state, e . Γ_{ev} is the vibronic homogeneous line width. The summation in eq 9 is over all molecular excited states $|ev\rangle$ except for the ground state. The Raman transition occurs between vibrational levels m and n of the ground electronic state, g . This expression predicts that the Raman intensity will increase as resonance is approached. In normal Raman scattering, numerous electronic transitions contribute to the Raman intensity; the contribution of each transition is weighted by its oscillator strength, the relevant Franck-Condon factors and the energy terms in the denominator. Given similar transition moments, the electronic transition closest to the excitation frequency should contribute most.

Symmetric vibrations are enhanced in strongly allowed electronic transitions by an A -term mechanism in which the scattered intensity is specified by the Franck-Condon overlap factors.

$$A = \sum_e [\langle g|R_\sigma|e\rangle\langle e|R_\rho|g\rangle] \sum_{\nu} \frac{\langle m|\nu\rangle\langle \nu|n\rangle}{\nu_{ev} - \nu_m - \nu_0 - i\Gamma_{ev}} \quad (10)$$

The intense symmetric tryptophan vibrational modes at 760, 1009, 1345, and 1550 cm^{-1} are expected to be mainly enhanced via the A -term mechanism. The depolarization ratios observed with 235-nm excitation of 0.30 ± 0.04 , 0.38 ± 0.05 , and 0.35 ± 0.05 for the 1009-, 1345-, and 1550- cm^{-1} vibrations,³ respectively, indicate that the resonant electronic transition to the B_b state is linearly polarized and not degenerate, and therefore, one diagonal element of the polarizability tensor dominates. In the case of the 760- cm^{-1} band the depolarization ratio of 0.26 ± 0.04 suggests a contribution from additional tensor elements, which we show may derive from a contribution from the B_a state (vide infra).

The measured resonance Raman excitation profiles (RREP's) of the 760-, 1009-, 1345-, and 1550- cm^{-1} bands displayed in Figure 3 show maxima at 224 nm, which are shifted by 4 nm to longer wavelengths from the B_b absorption maximum at 220 nm. This red shift could result partially from destructive interference due to preresonance enhancement by the B_a transition at ca. 195 nm. We estimated the likely influence of destructive interference between these transitions by calculating Raman intensity profiles based on eq 10 and the estimated values of Γ_{ev} and the oscillator strength, obtained from the observed absorption spectrum. The large line widths observed for upper singlet states of polyatomic molecules in the condensed phase are a result of their fast T_2 relaxation processes due to the high density of states.^{36a,b} The estimated values of Γ_{ev} are 3400 and 1700 cm^{-1} for the B_a and B_b transitions, respectively, and the ratio of oscillator strengths is 1.31. The dotted lines in Figure 6 represent the profiles if the vibration were coupled to a single transition, i.e., to only the B_a transition or to only the B_b transition. The solid curve shows the behavior which would occur if a vibration were enhanced by both the B_a and B_b excited states, with numerators of the same sign for both electronic transitions. We ignore the detailed Franck-Condon overlap factor sign changes since we see no explicit absorption vibronic substructure. As expected, the calculated band profile (solid line Figure 6) displays destructive interference in the region between the two electronic transitions, which results in a 1-nm red shift of the B_b profile. We may overestimate Γ_{ev} in this calculation since the absorption bandwidths could have a large contribution from inhomogeneous broadening. A smaller Γ_{ev} would result in a higher degree of destructive interference for each homogeneously broadened B_a and B_b transition pair. The dashed line in Figure 6 represents a case when the numerators

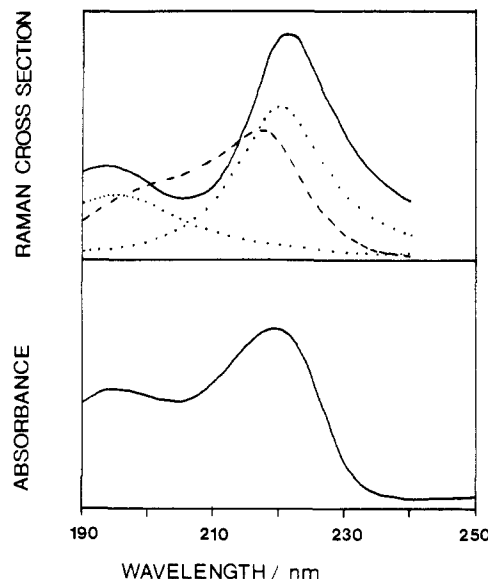


Figure 6. Calculations of Raman excitation profiles for A -term enhancement for a vibration enhanced by either the Trp B_a or B_b transition or both. The dotted lines show enhancement by the individual B_a and B_b transitions. The dashed and solid lines show the excitation profiles if both transitions contribute. Constructive interference (dashed line) results when the numerators of eq 11 have opposite signs for the two transitions. Destructive interference occurs when the numerations have the same sign. See text for details.

are of opposite sign for the two transitions. This leads to constructive interference in the region between the two transitions. Clearly this profile does not fit our experimental data. We note that if the B_a and B_b transitions were exactly perpendicular then no destructive interference would occur. Calculations^{15,20} suggest that, while the transitions are not perpendicular, they have a large angle between them.

Obviously, the 1-nm calculated red shift due to destructive interference is too small to account for our large 4-nm red shift of the experimental RREP's from the B_b absorption maximum. An excitation profile asymmetry which should signal strong destructive interference is not compellingly evident in the Figure 3 RREP. However, the initial decreases on the blue sides of the RREP maxima do appear to be asymmetric, but enhancement on the blue side of the B_b transition by vibronic bands probably masks the bulk of the destructive interference asymmetry. Destructive interference is evident from the cross sections observed with 207-nm excitation; excitation further to the UV such as at 200 nm demonstrates enhancement of the 760-, 1009-, and 1550- cm^{-1} bands by the B_a transition.⁴ It is unlikely that the Raman excitation profiles are red-shifted due to a false absorption maximum for the B_b transition caused by the overlap of the B_a transition. Deconvolution of these bands by Auer³⁷ reveals that the overlap of these transitions is insufficient to significantly shift the true B_b absorption maximum.

To obtain further information on the origin of the RREP red shift, we utilized the Raman transform methodology to calculate the RREP's of the tryptophan B_b transition. By assuming a Gaussian band shape, we deconvoluted the B_a transition from the tryptophan absorption spectrum; a Gaussian band shape was previously found to accurately model the B_a absorbance and CD band shapes.³⁷ We then applied the basic Condon resonance Raman transform methodology which utilized the Franck-Condon factor information presented in the absorption spectrum to calculate the RREP. The parameter ϕ_m is obtained from the B_b absorption band.³⁸⁻⁴⁴

$$\phi_m(\nu) = \frac{1}{\pi} P \int_0^\infty \frac{\sigma(x)}{x(x-\nu)} dx + \frac{i\sigma(\nu)}{\nu} \quad (11)$$

(35) Albrecht, A. C. *J. Chem. Phys.* **1961**, *34*, 1476.

(36) (a) Weiner, A. M.; Ippen, E. P. *Opt. Lett.* **1984**, *9*(2), 53; (b) Song, J. J.; Lee, J. H.; Levenson, M. D. *Phys. Rev. A* **1978**, *17*(4), 1439.

(37) Auer, H. E. *J. Am. Chem. Soc.* **1973**, *95*, 3003.

(38) Hassing, S.; Mortensen, O. S. *J. Chem. Phys.* **1980**, *73*(3), 1078.

Equation 11 is the fundamental equation of the transform theory where ϕ_m represents the excitation frequency dependent transform function for mode m . P is the Cauchy principal value of the integral, while $\sigma(x)$ and $\sigma(\nu)$ are absorbance cross sections at frequencies x and ν , in $\text{cm}^2/\text{molecule}$. The resonance Raman scattering polarizability amplitude for mode m is approximately equal to the difference between the transform function for mode m at excitation frequency ν minus the transform function evaluated at a frequency which is blue-shifted from that of ϕ_m by the frequency of the Raman active mode, m .

$$\alpha_m(\nu) \cong |\phi(\nu) - \phi(\nu - \nu_m)| \quad (12)$$

The total differential Raman cross section ($\text{cm}^2/(\text{molecule}\cdot\text{sr})$) is proportional to the square of the Raman scattering amplitude, and, for the case of a totally symmetric mode monitored at a 90° scattering geometry, may be expressed as

$$\left[\frac{d\sigma_m(\nu)}{d\Omega} \right]_{\parallel+\perp} = \text{constants} \times S_m |\phi(\nu) - \phi(\nu - \nu_m)|^2 \quad (13)$$

where S_m , the dimensionless Franck-Condon coupling strength for the m th normal mode contains the parameter ΔQ_m , representing the magnitude of the displacement of the equilibrium position of the excited-state potential energy surface for mode m relative to that of the ground state. S_m is expressed as

$$S_m = \left[\frac{k_m \Delta Q_m}{2F} \right]^2 = \left[\frac{\Delta Q_m}{2Q_m} \right]^2 \quad (14)$$

where Q_m is the rms displacement of the oscillator relative to its equilibrium geometry. F is the rms restoring force in the ground state for mode m , with k_m as the harmonic oscillator force constant. The constant in eq 13 contains a Boltzmann term which monitors the thermal average occupation of mode m , a ν^4 frequency-dependent term, and the square of the refractive index of the sample solution:

$$\text{constant} = 0.6 \times 10^{-17} \nu(\nu - \nu_m)^3 n^2 [(e^{h\nu_m/kT} - 1)^{-1} + 1] \quad (15)$$

Figure 3 displays the experimental RREP's of the tryptophan vibrational bands at 760, 1009, 1345, and 1550 cm^{-1} . The dotted lines in the figure show the RREP's of these bands calculated by using the basic Condon resonance Raman transform theory. The transform calculated RREP's show maxima at ca. 220 nm which closely coincide with the B_b transition absorption maximum. Thus, the transform theory expects a RREP maxima to coincide with the absorption band maxima.

We know from previous studies of aromatic molecules⁴⁴ that non-Condon sources are often important in strongly allowed transitions and can cause red shifts in the excitation profile maxima. Therefore, we applied the modified Raman transform theory which includes linear non-Condon coupling.

$$\left[\frac{d\sigma_m(\nu)}{d\Omega} \right]_{\parallel+\perp}^{\text{nc}} = \text{constant} \times S_m [(1 + C_m)\phi(\nu) - (1 - C_m)\phi(\nu - \nu_m)]^2 \quad (16)$$

where C_m is the non-Condon parameter for the Raman-active mode being investigated. The value of C_m is adjusted to achieve best fits with the experimental RREP. Increasing the C_m value for the 760- cm^{-1} band red shifts the transform profile ca. 1 nm from 221.9 nm ($C_m = 0.0$) to 223.1 nm ($C_m = 0.13$). C_m values greater than 0.13 do not result in further red shifts. Our best fit C_m values are 0.13, 0.13, 0.19, and 0.21 for the 760-, 1009-, 1345-, and 1550- cm^{-1} bands, respectively. As noted previously in pyrene

transform studies, C_m systematically increases as the vibrational frequency increases.⁴⁴

The line shapes of the non-Condon transform calculated RREP's give better fits to the experimental data than the basic Condon transform calculations. Based on the model Raman intensity profiles which demonstrate destructive interference, shown in Figure 6, and the Raman transform calculated excitation profiles which include non-Condon sources of intensity enhancement, shown in Figure 3 (solid line), we conclude that the red shifts of the experimental RREP's have contributions from both a destructive interference due to Raman intensity enhancement from the transition to the B_a excited state as well as from non-Condon sources of enhancement by the B_b transition. However, these two phenomena are not sufficient to explain the entire red shift.

The destructive interference between the B_a and B_b transitions creates a spectral window at ca. 205 nm for the examination of amide modes in proteins. The Raman cross sections of 0.42, 0.23, 0.31, and 0.51 barns/(molecule·sr) at 207 nm excitation for the 760-, 1009-, 1345-, and 1550- cm^{-1} bands, respectively, are 8-fold less than those at the profile maxima. Extrapolating these experimental Trp RREP's, we expect that the Raman cross sections will decrease even further as excitation extends further into the UV, possibly reaching a minimum at 205 nm.

We estimate from the experimental data of Song and Asher^{10a-c} and Copeland and Spiro⁴⁵ that the Raman cross section of the amide II mode is ca. 5 mbarn per peptide linkage with 205-nm excitation. This indicates that a protein containing 100 amino acids will show an amide II Raman band intensity comparable to that of a Trp residue. In fact, for the ca. 1400- cm^{-1} region we expect that the structure sensitive amide 2V band will be ca. 2-fold more intense than will the ca. 1345- cm^{-1} Trp band. Thus, a spectral window may be present for amide modes around 205 nm because the Trp modes are selectively deenhanced via destructive interference. Studies of amide modes in the protein backbone permit examination of protein secondary structure.¹⁰

The sharply peaked Trp excitation profile maxima allow selective enhancement of Trp residue in protein. The narrowness of the excitation profiles should allow selective enhancement of one Trp residue over another when the excitation profiles are shifted due to different environments. Different Trp environments in proteins are well known to result in ca. 5-nm absorption spectral shifts.⁴⁷ A 5-nm shift can translate into a 2-fold cross-section difference. We have recently documented Raman excitation profile shifts of aromatic amino acids in proteins such as myoglobin.⁴⁸ The different interresidue interactions for one Trp over another can be studied by examining the vibrational frequencies in the Raman spectra. These frequencies and band shapes depend upon interresidue interactions such as hydrogen bonding, for example. A comparison of these frequencies with excitation at the different excitation profile maxima of the different Trp will directly probe the environmental differences.

Conclusions

Our measured RREP's indicate that the 760-, 1009-, 1345-, and 1550- cm^{-1} tryptophan vibrational modes are strongly resonance enhanced with excitation in the B_b electronic transition. Sharp RREP maxima occur at 224 nm which will allow selective enhancement of Trp residues in proteins. The RREP show destructive interference on the high-energy side from the B_b electronic transition, and thus provides a spectral window at ca. 205 nm for the examination of amide modes of proteins. These findings combined with our previous extensive fundamental studies of the aromatic amino acids,^{1-3,11} amino acid dimers,⁴⁶ and amide modes¹⁰ detail the appropriate excitation wavelengths for selective en-

(39) Stallard, B. R.; Champion, P. M.; Callis, P. R.; Albrecht, A. C. *J. Chem. Phys.* **1983**, *78*(2), 712.

(40) Stallard, B. R.; Champion, P. M.; Callis, P. R.; Albrecht, A. C. *J. Chem. Phys.* **1984**, *80*(1), 70.

(41) Bangcharoenpaupong, O.; Schomacker, K. T.; Champion, P. M. *J. Am. Chem. Soc.* **1984**, *106*, 5688.

(42) Cable, J. R.; Albrecht, A. C. *J. Chem. Phys.* **1986**, *84*(4), 1969.

(43) Myers, A. B.; Mathies, R. A. In *Biological Applications of Raman Spectrometry*; Spiro, T. G., Ed.; Wiley: New York, 1987; Vol. II, p 1.

(44) Jones, C. M.; Asher, S. A. *J. Chem. Phys.* **1988**, *89*(5), 2649.

(45) Copeland, R. A.; Spiro, T. G. *Biochemistry* **1985**, *24*, 4960.

(46) Harmon, P. A.; Teraoka, J.; Asher, S. A. *J. Am. Chem. Soc.*, submitted for publication.

(47) Bailey, J. E.; Beaven, G. H.; Chignell, D. A.; Gratzen, W. B. *Eur. J. Biochem.* **1968**, *7*, 5.

(48) Larkin, P.; Teraoka, J.; Asher, S. A. *Biochemistry*, submitted for publication.

hancement of these species in proteins. The present studies were made using laser excitation powers which minimize Raman saturation and allow us to measure for the first time the total differential Raman cross sections of Trp.

Acknowledgment. We thank Paul A. Harmon for helpful discussions and assistance in the early stages of this work. We

gratefully acknowledge support of this work from NIH Grant 1R01GM30741-08. S.A.A. is an Established Investigator of the American Heart Association. This work was done during the tenure of an Established Investigatorship of the American Heart Association, Pennsylvania, affiliate.

Registry No. Trp, 73-22-3.

Theoretical Investigation of Chlorofluorocarbon Degradation Processes: Structures and Energetics of $\text{XC}(\text{O})\text{O}_x$ Intermediates ($\text{X} = \text{F}, \text{Cl}$)

Joseph S. Francisco,* Avery N. Goldstein, Zhuangjie Li, Yao Zhao,

Department of Chemistry, Wayne State University, Detroit, Michigan 48202

and Ian H. Williams

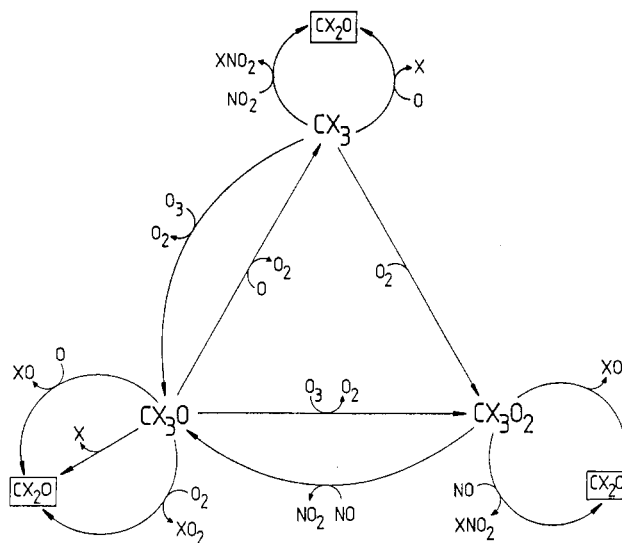
School of Chemistry, University of Bath, Bath, BA2 7AY, U.K. (Received: August 25, 1989; In Final Form: November 14, 1989)

Photodissociation of stratospheric chlorofluoromethanes leads to carbonyl dihalide CX_2O , whose further degradation is also initiated by a photodissociation step. The energetics of possible oxidation pathways involving XCO , $\text{XC}(\text{O})\text{O}$, and $\text{XC}(\text{O})\text{O}_2$ radicals have been investigated by calculations at the UMP2/6-31G* and PMP2/6-31G* levels of ab initio molecular orbital theory. In the absence of experimental thermochemical data, calculated heats of reaction are used in discussions of the possible involvement of these intermediates in reactions of atmospheric significance.

Introduction

It is generally accepted that a stratospheric chlorofluoromethane (CFM) undergoes UV photodissociation to yield a chlorine atom that participates in the ClO_x catalytic cycle;¹⁻³ less well understood is the subsequent fate of the trihalomethyl radical generated in the same process. We have embarked upon a theoretical survey of the mechanisms of oxidation of trihalomethyl radicals, to complement experimental studies of key reactions currently under way, and have suggested that the net result of the oxidation pathways for CX_3 depicted in Scheme I is the formation of stable halocarbonyl compounds CX_2O along with the release of halogen atoms.⁴⁻⁶ Recent in situ measurements have indeed confirmed the presence of CF_2O and CCl_2O in the stratosphere,^{7,8} thus providing indirect support for this view. Carbonyl dihalides CX_2O may themselves undergo UV photodissociation, yielding haloformyl radicals XCO and halogen atoms.⁹⁻¹¹ To aid the assessment of the possible oxidation pathways for XCO depicted in Scheme II, it is necessary to have knowledge of the heats of reaction for these various processes. Since experimental data are lacking, particularly for species $\text{XC}(\text{O})\text{O}_x$, we report here the results of ab initio quantum-chemical calculations for the energetics of chlorofluoromethane degradation reactions in order to comment upon

SCHEME I: Oxidation Pathways for CX_3 Radicals



their possible implications for stratospheric chemistry.

Methods and Results

The GAUSSIAN86¹² and CADPAC¹³ program were used to perform ab initio molecular orbital calculations with the 6-31G* bases¹⁴ for first-row atoms and the 6-31G* basis¹⁵ for chlorine. The geometry of each species (Table I) was optimized by using the

- (1) Cicerone, J. R. *Science* **1987**, 237, 35.
- (2) Wayne, R. P. *Chemistry of Atmospheres*; Clarendon Press: Oxford, 1985.
- (3) Sridharan, U. C.; Klein, F. S.; Kaufman, F. J. *Chem. Phys.* **1985**, 82, 592.
- (4) Francisco, J. S.; Li, Z.; Williams, I. H. *Chem. Phys. Lett.* **1987**, 140, 531.
- (5) Francisco, J. S.; Williams, I. H. *Int. J. Chem. Kinet.* **1988**, 20, 455.
- (6) Francisco, J. S.; Williams, I. H. *Proc. 16th Annu. Mtg. Natl. Org. Black Chem. Chem. Eng., Chicago, IL, 1989*.
- (7) Rinsland, C. P.; Zander, R.; Brown, L. R.; Farne, C. B.; Park, J. H.; Norton, R. H.; Russel, J. M.; Raper, O. F. *Geophys. Res. Lett.* **1986**, 13, 769.
- (8) Wilson, S. R.; Crutzen, P. J.; Schuster, G.; Griffith, D. W. T.; Helas, G. *Nature* **1988**, 334, 689.
- (9) Rowland, F. S.; Molina, M. J. *Res. Geophys. Space Phys.* **1975**, 13, 1.
- (10) Sze, N. D. *Geophys. Res. Lett.* **1978**, 5, 781.
- (11) Simonaitis, R. In *Proceedings of the NATO ASI on Atmospheric Ozone*; Rep. FAA-EE-80-20, Aikin, A. C., Ed.; Washington, DC, 1980; pp 501-515.

- (12) Frisch, M. J.; Binkely, J. S.; DeFrees, D. J.; Raghavachari, K.; Schlegel, H. B.; Whiteside, R. A.; Fox, D. J.; Martin, R. L.; Fluder, E. M.; Melius, C. F.; Kahn, L. R.; Stewart, J. J. P.; Bobrowicz, F. W.; Pople, J. A. GAUSSIAN86, Carnegie-Mellon Quantum Chemistry Publishing Unit: Pittsburgh, PA, 1984.
- (13) Amos, R. D.; Rice, J. E. CADPAC4.0, University of Cambridge, Cambridge, 1987.
- (14) Binkley, J. S.; Pople, J. A.; Hehre, W. J. *J. Am. Chem. Soc.* **1980**, 102, 939. Hariharan, P. C.; Pople, J. A. *Theor. Chim. Acta* **1973**, 28, 213.
- (15) Francl, M. M.; Pietro, W. J.; Hehre, W. J.; Binkley, J. S.; Gordon, M. S.; DeFrees, D. J.; Pople, J. A. *J. Chem. Phys.* **1982**, 77, 3654.